Front. Earth Sci. China 2009, 3(1): 118–128
DOI 10.1007/s11707-009-0012-x

RESEARCH ARTICLE

Estimation of winter wheat biomass based on remote sensing data at various spatial and spectral resolutions

Yansong BAO (✉)[1,2,3], Wei GAO[2,3], Zhiqiang GAO[2,3,4]

1 School of Atmospheric Physics, Nanjing University of Information Science & Technology, Nanjing 210044, China
2 USDA UV-B Monitoring and Research Program, Natural Resource Ecology Laboratory, Colorado State University, Fort Collins, CO80521, USA
3 Key Lab of Geographic Information Science, East China Normal University, Shanghai 200062, China
4 Institute of Geographical Sciences and Natural Resources Research, Chinese Academy of Sciences, Beijing 100101, China

Abstract Biomass can indicate plant growth status, so it is an important index for plant growth monitoring. This paper focused on the methodology of estimating the winter wheat biomass based on hyperspectral field data, including the LANDSAT TM and EOS MODIS images. In order to develop the method of retrieving the wheat biomass from remote sensed data, routine field measurements were initiated during periods when the LANDSAT satellite passed over the study region. In the course of the experiment, five LANDSAT TM images were acquired respectively at early erecting stage, jointing stage, earring stage, flowering stage and grain-filling stage of the winter wheat, and the wheat biomass was measured at each stage. Based on the TM and MODIS images, spectral indices such as NDVI, RDVI, EVI, MSAVI, SIPI and NDWI were calculated. At the same time, the hyperspectral field data was used to compute the normalized difference in spectral indices, red-edge parameters, spectral absorption, and reflection feature parameters. Then the correlation coefficients between the wheat biomass and spectral parameters of the experiment sites were computed. According to the correlation coefficients, the optimal spectral parameters for estimating the wheat biomass were determined. The best-fitting method was employed to build the relationship models between the wheat biomass and the optimal spectral parameters. Finally, the models were used to estimate the wheat biomass based on the TM and MODIS data. The maximum RMSE of estimated biomass was 66.403 g/m^2.

Keywords LANDSAT TM, EOS MODIS, biomass retrieval, spectral indices

Received August 30, 2008; accepted October 30, 2008

E-mail: ysbao@hotmail.com

1 Introduction

Crop biomass is the major index which can show crop growth. N availability is an important determinant factor of crop growth and productivity (Van Keulen et al., 1989). Under non-water stress growth condition, the N status of a crop is the major factor controlling the rate of biomass accumulation (Jensen et al., 1990). The reflectance spectra of all types of vegetation in the 0.4–2.4 μm spectral region are remarkably similar. In near-infrared wavelengths, there is a high reflectance as a result of leaf scattering, while in visible wavelengths (0.4–0.7 μm) reflectance is low because of chlorophyll absorption (Curran, 1989). Research has shown that wheat total nitrogen has high correlation with leaf area index (LAI) and chlorophyll (Bao, 2006). Thus, vegetation reflectance can be used to monitor crop growth, and estimate the plant biomass.

Numerous studies have been conducted, regarding the potential of remote sensing technology as an effective estimator of plant biomass. These studies have focused on forest biomass estimation by employing the visible, synthetic aperture radar (SAR), and lidar data. In addition, studies have also considered crop biomass estimation. Gitelson et al. (2003) used MODIS reflectance to estimate the maize green leaf biomass. Svoray (2002) introduced the water-cloud model into SAR data to estimate the aerial aboveground biomass of herbaceous vegetation. Del Frate conducted some experiments to estimate the sunflower biomass using a neural network algorithm based on radar data. Jin estimated the wheat and oat biomass based upon active/passive remote sensing data at microwave bands. Liu et al. (2002) retrieved the wheat biomass from measured 1.4 and 10.65 GHz brightness temperatures.

The focus of this paper is estimating the winter wheat biomass based on LANDSAT TM 5 and EOS MODIS images. In section 2, the methods and data processes are

outlined. Section 3 is a discussion of the experimental results and conclusions are summarized in Section 4.

2 Materials and methods

2.1 Experimental site

The experimental area was located in the suburban counties of Beijing city, China, with arid and semi-arid environment. There were 25 and 27 winter wheat fields selected from Chanping, Shunyi and Tongxian, respectively in 2004 and 2005 (Fig. 1). These fields were located between 115°58′–116°50′ E longitude and 39°30′–40°33′ N latitude. Each field was a minimum of 4 ha and planted with the same variety under the same sowing, fertilization, and irrigation procedures. The largest latitudinal distance among these fields was 53 km, and the largest longitudinal distance was 47 km. The study area was flat, and fine clay loam was the predominant soil texture.

2.2 Data acquisition

Field experiments were conducted on days when the satellite LANDSAT 5 passed over Beijing. We acquired the winter wheat biomass at eight growth stages for 2004–2005. These eight growth stages were early erecting stage, late erecting stage, jointing stage, booting stage, earring stage, flowing stage, grain-filling stage and maturing stage.

2.2.1 Canopy spectral measurements

All canopy spectral measurements were taken from a height of 50 cm above canopy, under clear blue sky between 10:00 and 14:00 in Beijing Local Time, using an ASD FieldSpec Pro spectrometer (Analytical Spectral Devices, Boulder, CO, USA) fitted with 25° field of view fiber optics, which function in the 350–2500 nm spectral region with a spectral resolution of 3 nm at 700 nm and 10 nm in the 1400–2500 nm range, and with a sampling interval of 1.4 nm between 350 and 1050 nm, and 2 nm between 1050 and 2500 nm. Measurements over a 40 cm×40 cm $BaSO_4$ calibration panel were used for calculation of reflectance. Vegetation and panel radiance measurements were taken by averaging 20 scans at optimized integration time with due care for dark current correction at every spectral measurement (Huang et al., 2004).

2.2.2 Satellite images

There were three LANDSAT TM images acquired on April 1, April 17 and May 19, 2004 at winter wheat's erecting stage, jointing stage and flowering stage, respectively. In 2005, two images were acquired on May 6 and May 22 at the earring stage and grain-filling stage, respectively. Spatial resolution for all TM images was 30 m.

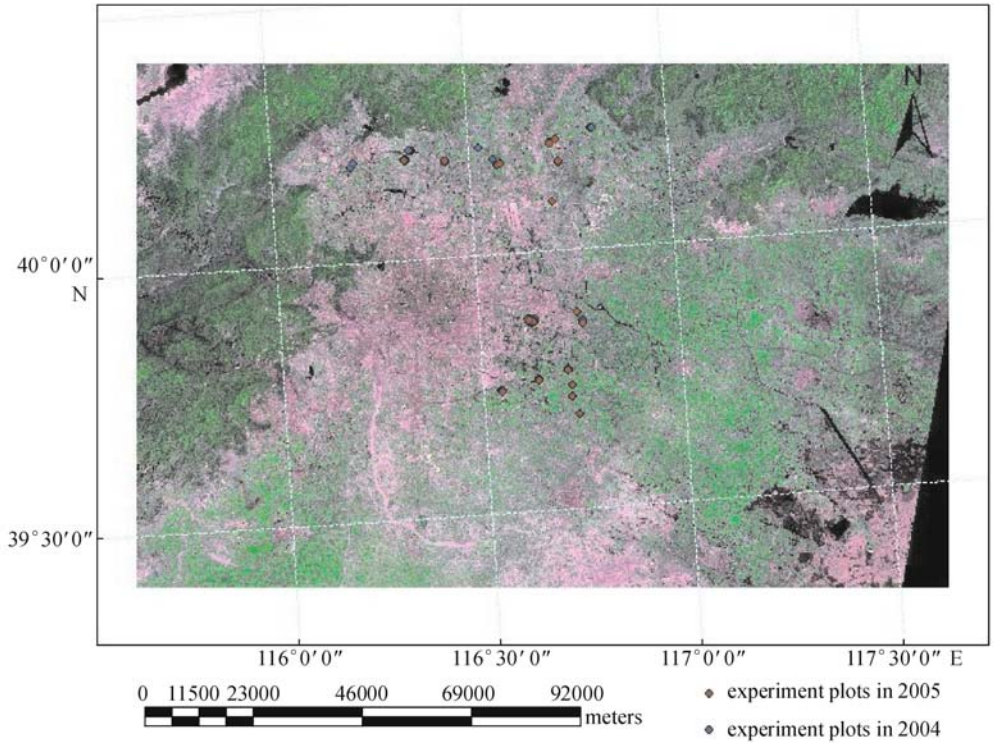

Fig. 1 Experimental plots of Beijing in 2004 and 2005

MODIS Surface Reflectance images of eight growth stages were downloaded from the Land Process Distributed Active Archive Center (LPDAAC). The MOIDIS images were 8-day gridded level-3 products with a spatial resolution of 500 m per pixel, and in the sinusoidal projection. For this product, corrections were made for the effect of atmospheric gases and aerosols.

2.2.3 Biomass

At each site, a 0.6 m×0.5 m wheat sample was taken and sealed in a plastic bag. The fresh samples were taken back, then oven-dried at 60° until a constant weight was reached. The wheat biomass was calculated by dividing dry weight by sample area.

2.2.4 Image pre-processing

Coarse geometric correction of TM images was carried out based on a 1∶10000 digitized raster map, and precise geometric correction was completed using the GPS ground control points. The geometric correction precision was better than one pixel.

The Empirical Line (EL) calibration method was employed for LANDSAT TM atmospheric correction. A reservoir and another concrete airdrome were selected as the dark and bright regions in the image for use in the EL calibration. The field reflectance spectra of the reservoir and concrete airdrome were measured by an ASD FieldSpec Pro spectrometer when the TM image was acquired. The image digital number (DN) spectra of the dark and bright regions were extracted from the images according to the GPS value recorded when the field spectra were collected. A linear regression was calculated between the field reflectance spectra and the image spectra. The regression line was used to predict the surface reflectance spectra for each pixel from its original image spectrum.

MODIS Image geo-correction procedure included mosaic, re-projection and subset. These processes were completed by the software of MRT. Scale factors of reflectance data were obtained from the website of data center, and were used to calculate the ground truth reflectance.

3 Results and analyses

3.1 Relating biomass to hyperspectral data

Many studies have employed hyperspectral data to estimate the plant biophysical and biochemical parameters, including leaf area index (Vuolo et al., 2008), biomass (Ge et al., 2007), chlorophyll content (Wu et al., 2008), nitrogen (Tilling et al., 2007) and water content (Colombo et al., 2008). In this study, spectral reflectance (Starks et al., 2008), spectral indices (Zarco-Tejada et al., 2005), red edge parameters (Cho et al., 2008), and spectral reflection and absorption parameters (Liu, 2002) were widely used.

3.1.1 Normalized difference spectral indices

Normalized difference spectral index is formulated as follows:

$$NDSI_i = \frac{|R_i(\mathrm{B1}) - R_i(\mathrm{B2})|}{R_i(\mathrm{B1}) + R_i(\mathrm{B2})}, \quad (1)$$

where i is the subscript of Normalize Difference Spectral Index, R_i (B1) and R_i (B2) are the reflectance of B1 and B2 spectral band. In this study, 7 NDSIs were used to estimate the winter wheat biomass. The wavelengths of B1 and B2 are listed in Table 1 (Liu, 2002).

Table 1 Wavelengths of B1 and B2

index	1	2	3	4	5	6	7
B1/nm	560	670	890	920	857	820	820
B2 /nm	670	890	980	980	1210	1650	2200

3.1.2 Vegetation Red-edge position (REP)

As for hyperspectral remote sensing technology, vegetation Red-edge spectral characteristics were usually emphased (Horler et al., 1983; Baret et al., 1992; Curran et al., 1995; Clevers et al., 2002). The red-edge represents the region of abrupt change in leaf reflectance between 680 nm and 780 nm caused by the combined effects of strong chlorophyll absorption in the red and leaf internal scattering in the near-infrared wavelengths (Gates et al., 1965). Increases in the amount of chlorophyll results in a broadening of the major chlorophyll absorption feature centered around 680 nm (Buschmann and Nagel, 1993; Dawson and Curran, 1998) causing a shift in the slope and REP towards longer wavelengths (Collins et al., 1977; Clevers et al., 2002).

There are many algorithms to calculate Red-edge spectral features (Liu et al., 2004; Bonham-Carter, 1988; Miller et al., 1990; Railyan and Korobov, 1993; Dawson and Curran, 1998). The inverted-Gaussian (IG) model (Bonham-Carter, 1988; Miller et al., 1990), which represents the reflectance red edge well, is defined as follows:

$$R(\lambda) = R_s - (R_s - R_0)\exp\left(\frac{-(\lambda_0 - \lambda)}{2\sigma^2}\right), \quad (2)$$

where R_s is the maximal spectral reflectance, R_0 is the minimal spectral reflectance, λ_0 is the wavelength where the reflectance is the minimum, and σ is the Gaussian function deviation parameter. σ is the key parameter to describe the Red-edge shape. If σ is larger, the Red-edge

reflectance increases more rapidly and the Red-edge becomes steeper.

The Red-edge position, λ_p, is defined by the wavelength of the maximum in the first derivative of Gaussian function (Miller et al., 1990).

$$\lambda_p = \lambda_0 + \sigma. \quad (3)$$

This expression is graphically illustrated in Fig. 2, where the IG model was fitted to the red edge reflectance in 685–780 nm region using the inverted-Gaussian model (Miller et al., 1990).

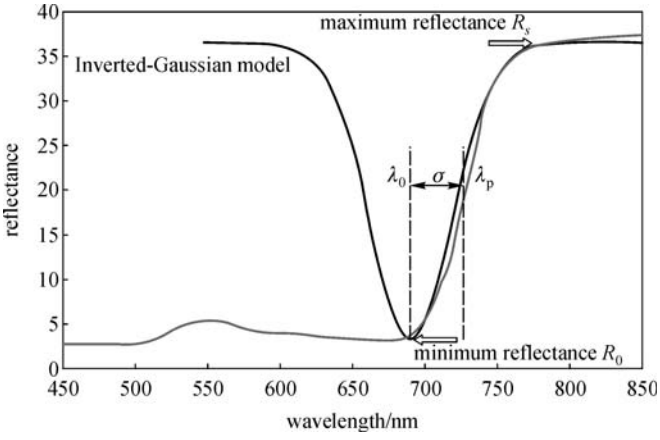

Fig. 2 Inverted Gaussian reflectance model and red-edge parameters

3.1.3 Spectral absorption and reflection parameters

Spectral absorption and reflection parameters, such as absorption peak depth, absorption region spectral area, normalized absorption peak depth, reflection peak depth, reflection region spectral area and normalized reflection peak depth, can be used to estimate the plant biophysical and biochemical parameters (Liu, 2002). Liu (2002) defined these spectral absorption and reflection parameters and used them to inverse the winter wheat biophysical and biochemical parameters.

3.1.4 Biomass estimation models

According to the definition of the hyperspectral parameters, these parameters were calculated, and the correlation coefficients between the hyperspectral parameters and biomass were computed. The correlation coefficients are shown in Table 2.

The spectral parameters, which have the maximum values, are used to build the biomass estimation models by the best-fitting method. The biomass retrieval models are shown in Table 3.

Table 2 Correlation coefficients between the biomass and hyperspectral parameters

reflectance and spectral parameters	4/3/2005	4/15/2004	4/21/2005	5/8/2005	5/18/2004	5/22/2005	6/2/2004
455	−0.627	−0.706	−0.741	−0.35	0.198	−0.239	−0.144
550	−0.566	−0.731	−0.665	−0.254	0.205	−0.29	−0.001
680	−0.753	−0.765	−0.796	−0.515	0.038	−0.296	−0.527
980	0.627	0.364	0.385	0.214	0.246	0.132	0.389
1090	0.644	0.459	0.43	0.319	0.268	0.195	0.388
1200	0.375	−0.054	0.095	−0.068	0.169	−0.063	0.156
1285	0.38	−0.048	0.095	−0.038	0.141	−0.055	0.135
1468	−0.686	−0.717	−0.748	−0.611	0.004	−0.34	−0.598
1685	−0.468	−0.629	−0.581	−0.454	0.015	−0.313	−0.461
2200	−0.649	−0.713	−0.741	−0.619	0.045	−0.334	−0.602
[670,890]	0.85	0.799	0.797	0.624	0.091	0.308	0.538
[890,980]	0.837	0.906	0.823	0.725	0.535	0.489	0.679
[920,980]	0.844	0.909	0.818	0.722	0.486	0.49	0.647
[857,1210]	0.825	0.884	0.823	0.743	0.459	0.465	0.692
[820,1650]	0.826	0.849	0.799	0.746	0.333	0.396	0.657
[820,2200]	0.81	0.799	0.785	0.733	0.161	0.358	0.643
REP	0.71	0.894	0.686	0.575	−0.012	0.392	0.291
Lo	0.815	0.82	0.76	0.467	0.25	0.335	0.481
Lwidth	−0.775	−0.493	−0.7	0.557	−0.522	0.015	−0.615
depth 672	0.849	0.785	0.788	0.622	0.122	0.298	0.563
area 672	0.855	0.828	0.798	0.568	0.099	0.333	0.552
ND 672	−0.821	−0.855	−0.772	−0.518	−0.052	−0.363	−0.409

(*Continued*)

reflectance and spectral parameters	4/3/2005	4/15/2004	4/21/2005	5/8/2005	5/18/2004	5/22/2005	6/2/2004
depth 980	0.862	0.912	0.803	0.736	0.461	0.492	0.631
area 980	0.861	0.912	0.802	0.743	0.411	0.504	0.64
ND 980	0.286	0.433	−0.311	−0.649	0.293	−0.24	0.122
depth 1190	0.871	0.892	0.788	0.769	0.252	0.444	0.571
area 1190	0.868	0.894	0.79	0.768	0.253	0.443	0.587
ND 1190	−0.536	−0.777	−0.808	−0.698	−0.117	−0.393	−0.571
depth 1450	0.792	0.761	0.761	0.706	0.109	0.313	0.578
area 1450	−0.767	−0.786	−0.333	0.052	−0.464	0.165	−0.554
ND 1450	−0.107	0.483	0.501	0.401	0.167	0.365	0.493
P_depth 560	−0.401	−0.472	−0.742	−0.63	−0.063	−0.126	−0.349
PND 560	0.797	0.718	0.823	0.512	0.099	0.145	0.63
P_area 560	0.792	0.704	0.826	0.56	0.098	0.141	0.622
P_depth 920	0.738	0.728	0.738	0.41	0.488	0.259	0.652
PND 920	0.842	0.883	0.796	0.721	0.381	0.515	0.503
P_area 920	0.846	0.865	0.79	0.728	0.302	0.542	0.436
P_depth 1100	0.499	−0.672	−0.071	−0.025	−0.297	−0.033	−0.486
PND 1100	0.862	0.896	0.789	0.77	0.24	0.475	0.585
P_area 1100	0.864	0.897	0.787	0.765	0.277	0.462	0.591
P_depth 1280	−0.557	−0.718	−0.764	−0.639	0.216	−0.172	−0.288
PND 1280	0.817	0.786	0.75	0.749	−0.066	0.34	0.522
P_area 1280	0.78	0.766	0.777	0.662	−0.308	0.189	0.441
P_depth 1690	−0.08	−0.488	−0.659	−0.411	−0.227	−0.399	−0.545
PND 1690	0.734	0.747	0.751	0.546	0.112	0.227	0.65
P_area 1690	0.719	0.74	0.761	0.548	0.162	0.248	0.658
P_depth 2230	−0.562	−0.301	−0.469	−0.544	0.512	−0.27	−0.351
PND 2230	0.519	0.635	0.748	0.314	0.449	0.031	0.369
P_area 2230	0.54	0.662	0.762	0.385	0.379	0.066	0.433

Note: $r_{(0.05,26)}= 0.381$, $r_{(0.01,26)}= 0.487$. the description of the spectral parameters can be found in the reference paper 20

Table 3 Biomass retrieval model based on the hyperspectral parameters at different growth stages

growth stage	model	pptimal spectral parameter	R^2
late erecting stage	$y = 884.96x + 9.868$	depth 1190	0.759
jointing stage	$y = 43.571x - 42.686$	area 980	0.833
booting stage	$y = 604.11x + 85.259$	P_area 560	0.682
earring stage	$y = 3257.8x - 159.16$	PND 1100	0.593
flowering stage	$y = 6611.9x + 125.26$	[890,980]	0.286
grain-filling stage	$y = 105.88x - 322.48$	P_area 920	0.294
maturing stage	$y = 2608.2x + 234.3$	[857,1210]	0.479

3.2 Relating biomass to TM data

3.2.1 The optimal spectral indices for estimation of the biomass

Numerous studies have successfully related various spectral indices using ratios of red and infrared reflectance with crop vigor, condition, and biomass. In this study, six spectral indices were employed, as shown in Table 4. These indices were related to crop LAI, biomass, pigments and plant water content.

As only five TM images were acquired, it was difficult to search the optimal spectral indices to retrieve the wheat biomass during the whole growth period. However, the

field measurements could provide the hyper-spectral data of wheat during the whole growth period. Combining the hyper-spectral data and TM sensors' spectral responding functions, the TM spectral reflectance was simulated. Using the simulated reflectance, the spectral indices of the experiment sites were acquired at the eight stages. These data were enough to research the retrieval of the wheat biomass during the whole growth period.

In order to retrieve the wheat biomass, we needed to search the optimal indices from these spectral indices. Based on the simulated reflectance, the spectral indices were calculated. Then the correlation coefficients between the spectral indices and biomass of the experiment sites were computed. Correlation analysis results are shown in Table 5.

As shown in Table 5, all spectral indices had significant correlation at 1% level with the biomass at erection stage. The spectral index NDWI had the highest correlation with the biomass at jointing, booting, earring, grain-filling, and maturing stages. At flowering stage, EVI had the highest correlation with the biomass compared to other spectral indices.

In order to validate the analysis result based on the simulated data, the five TM image data were used. The same analysis method was employed to the TM data. The correlation coefficients between the biomass and spectral indices are shown in Table 6.

Table 6 shows that the optimal indices were NDVI, NDWI, NDWI, EVI and NDWI at the five stages, respectively. This conclusion was consistent with the analysis result based on the simulated data. Therefore, the simulated data could be used to study the optimal spectral indices for retrieving biomass.

Table 5 shows that NDWI had the highest correlation coefficients with the biomass at the five stages. Compared with other spectral indices, NDWI had better correlation with the biomass at the other three stages. Considering the simplicity of the optimal indices, NDWI was confirmed to be the optimal index.

Due to the definition, NDWI was the optimal index of

Table 4 Spectral indices used in this paper

acronym	index	equation	reference
NDVI	normalized difference vegetation index	NDVI =(TM4—TM3)/(TM4 + TM3)	Rouse et al., 1974
RDVI	renormalized difference vegetation index	RDVI =(TM4—TM3)/SQRT(TM4 + TM3)	Rougean & Breon, 1995
MSAVI	modified soil-adjusted vegetation index	(2TM4 + 1—SQRT((2TM4 + 1)∧2–8(TM4—TM3)))/2	Qi et al., 1994
EVI	enhanced vegetation index	2.5(TM4—TM3)/(1 + TM4 + 6TM3–7.5TM1)	Huete et al., 1996
SIPI	structure insensitive pigment index	SIPI =(TM4—TM1)/(TM4—TM3)	Peñuelas et al., 1995
NDWI	normalized difference water index	NDWI =(TM4—TM5)/(TM4 + TM5)	Gao, 1996

Table 5 The correlation coefficients of wheat biomass and spectral indices based on the simulated data

Date	4/1/2004	4/3/2005	4/15/2004	4/21/2005	5/8/2005	5/18/2004	5/22/2005	6/2/2004
phenophase	early erecting stage	late erecting stage	jointing stage	booting stage	earring stage	flowering stage	grain-filling stage	maturing stage
NDVI	0.888	0.852	0.806	0.796	0.606	0.091	0.312	0.551
RDVI	0.888	0.869	0.792	0.739	0.518	0.305	0.294	0.593
EVI	0.888	0.858	0.780	0.731	0.491	0.332	0.292	0.621
MSAVI	0.891	0.868	0.784	0.731	0.492	0.325	0.289	0.606
SIPI	−0.782	−0.816	−0.734	−0.729	−0.577	−0.192	−0.287	−0.500
NDWI	0.883	0.828	0.842	0.797	0.745	0.317	0.390	0.693

Note: $r_{(0.05,25)}$= 0.396, $r_{(0.01,25)}$= 0.505, $r_{(0.05,27)}$= 0.381, $r_{(0.01,27)}$= 0.487

Table 6 Correlation coefficients of wheat biomass and spectral indices based on TM data

date	4/1/2004	4/15/2004	5/6/2005	5/19/2004	5/22/2005
phenophase	early erecting stage	jointing stage	earring stage	flowering stage	grain-filling stage
NDVI	0.847	0.614	0.782	0.312	0.342
RDVI	0.814	0.629	0.748	0.492	0.389
EVI	0.829	0.787	0.706	0.641	0.330
MSAVI	0.804	0.622	0.752	0.496	0.390
SIPI	−0.762	−0.757	−0.638	−0.637	−0.252
NDWI	0.842	0.803	0.833	0.579	0.544

biomass estimation. In our study, NDWI was composed of TM reflectance at the near infrared and short infrared band. TM near infrared reflectance could depict the greenness of vegetation, and its shortwave infrared reflectance could denote the water content information of vegetation. Vegetation biomass has a direct relation with greenness and an indirect relationship with water content. Therefore, NDWI was selected as the optimal spectral index to estimate the biomass.

The correlation coefficients between NDWI and the biomass decreased as wheat grew before the flowering stage and increased after flowering stage. During the flowering stage, the correlation coefficient was minimal. At early growth stage, the sensitivity of wheat field reflectance spectrum to the biomass was the highest, and the sensitivity decreased with wheat growth. The sensitivity was the lowest during the flowering stage because the wheat canopy was the most flourishing. At this stage, the sensitivity approached the minimum value. After the flowering stage some leaves began to fall, therefore, the sensitivity increased.

3.2.2 The biomass estimation models

Using the best-fitting method to build the biomass estimation model, the wheat biomass estimation models were developed and illustrated in Figs. 3–7. Figures 3–7 show that the accuracies of biomass estimation were high during the vegetative stage from the erecting to the earring stage. Using the best-fitting method, a biomass estimation model was built for the vegetative stage and the resulting model is shown in Fig. 8.

3.3 Relating biomass to MODIS data

3.3.1 MODIS optimal spectral indices for biomass estimation

In searching the optimal spectral indices, we used the MODIS data on the days when the biomass was measured at the experiment fields. First, the correlation coefficients between the biomass and spectral indices were calculated, and the results are shown in Table 7.

The optimal index was SIPI at erecting and jointing stages. Near infrared reflectance was the optimal index from booting to grain-filling stages. During the maturing stage, shortwave infrared reflectance was the optimal index and furthermore near infrared reflectance had the highest correlation coefficient with the biomass at the vegetative stage. A similar result was found that the correlation between the biomass and spectral indices was the lowest during the flowering stage.

At erecting and jointing stages, wheat canopy could not cover the fields completely. Therefore, crop geometric structure had an apparent effect on the relation between the biomass and spectrum. As SIPI could weaken crop structure effect, SIPI had higher correlation with the biomass.

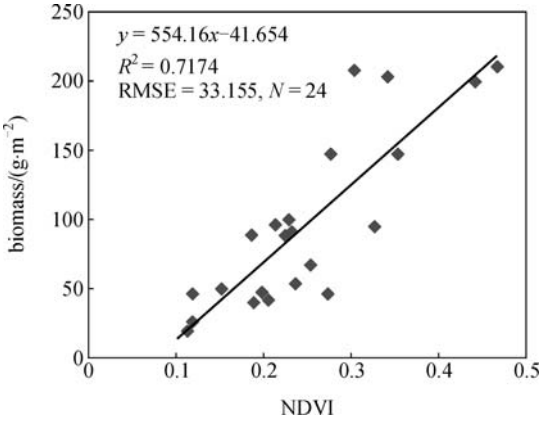

Fig. 3 Relation between NDVI and biomass on April 1, 2004 (early erecting stage)

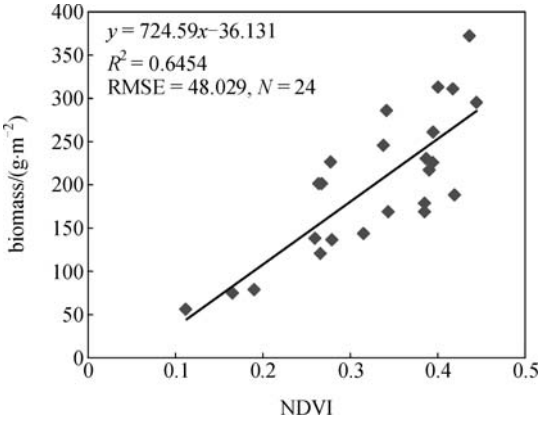

Fig. 4 Relation between NDVI and biomass on April 17, 2004 (jointing stage)

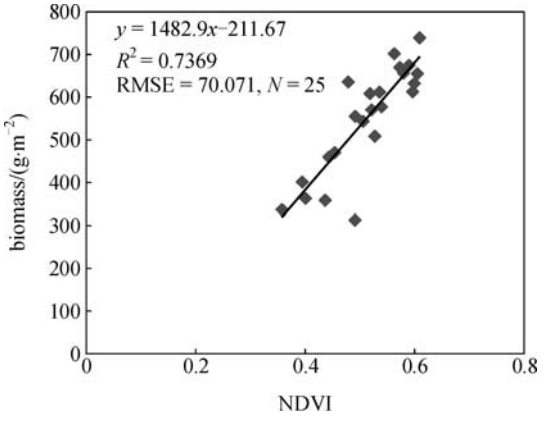

Fig. 5 Relation between NDVI and biomass on May 6, 2005 (earring stage)

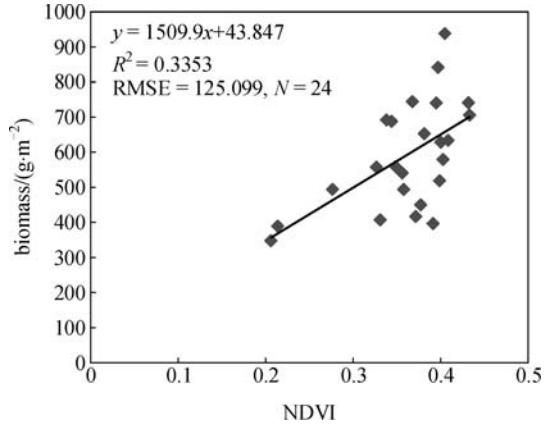

Fig. 6 Relation between NDVI and biomass on May 19, 2004 (flowing stage)

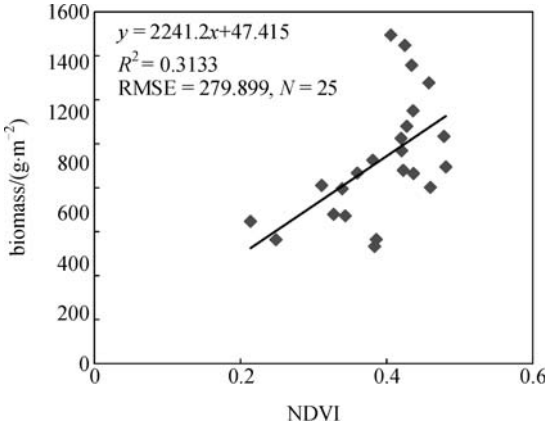

Fig. 7 The relation between NDVI and biomass on May 22, 2004 (grain-filling stage)

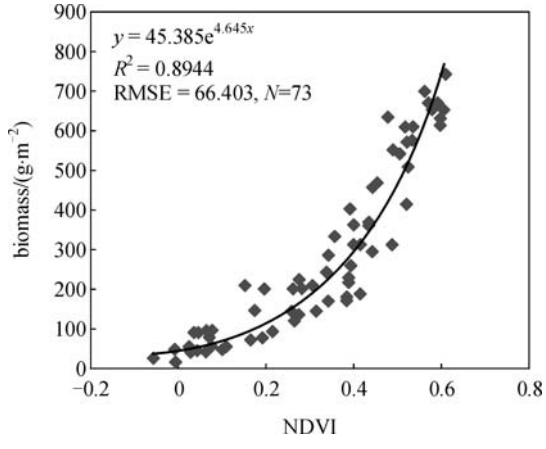

Fig. 8 The relation between NDVI and biomass on vegetative stage

The analysis results for TM data showed that NDWI had higher correlation with the biomass at most stages. However, this conclusion was not found when using MODIS data. The main reason was MODIS shortwave infrared sensor's SNR was lower.

3.3.2 Biomass estimation model

As MODIS eight-day reflectance had eliminated the effects of cloudy and view angle, it was used to build a wheat biomass estimation model at vegetative stage (Fig. 9).

3.4 Application of the biomass estimation models

The previous sections showed that the wheat biomass could be retrieved during the vegetation stage based on the TM or MODIS images. The biomass estimation model in Fig. 8 was used to analyze TM images during the vegetative stage and the biomass of the experimental region can be seen in Figs. 10–12. We used the model in Fig. 9 to calculate the plant biomass of wheat fields based on MODIS images (Figs. 13–15)

4 Conclusion and discussion

Conclusions could be drawn based on previous correlation analyses and biomass estimation results:

(1) During the whole growth stage of winter wheat, the correlation coefficients between winter wheat biomass and hyperspectral parameters were higher before the flowering stage. Among these hyperspectral parameters, spectral absorption and reflection feature parameters had the highest correlation with the biomass. Therefore, based on the optimal spectral parameters, the biomass estimation models were built. The R^2 values of these models were higher than 0.5 before the flowering stage.

(2) With regard to wheat biomass estimation based on TM images, NDWI was a proper spectral index. The reason was NDWI could reflect plant greenness and water content, which was very important to biomass accumulation. The correlation coefficients between the biomass and NDWI increased during the vegetative stage and decreased during the reproductive stage. During the flowering stage, the correlation coefficient was minimal.

(3) While the correlation coefficients between biomass and NDWI were low during the reproductive stage, only the data from the vegetative stage were used to fit the wheat biomass estimation model. The relation between NDWI and wheat biomass could be described by a logarithm equation. The wheat biomass estimation model had a R^2 of 0.8944 and the estimated biomass had a RMSE of 66.403 g/m^2.

(4) With respect to wheat biomass estimation based on MODIS images, SIPI was the optimal index for retrieval of the biomass at erecting and jointing stages and near infrared reflectance was the optimal index for the other stages. NDWI was not the optimal index because MODIS shortwave infrared sensor's SNR was low. The correlation

Table 7 Correlation coefficient between biomass and MODIS spectral indices

date	4/1/2004	4/3/2005	4/15/2004	4/21/2005	5/8/2005	5/18/2004	5/22/2005	6/2/2004	vegetative stage
phenophase	early erecting stage	late erecting stage	jointing stage	booting stage	earring stage	flowering stage	grain-filling stage	maturing stage	
MODIS1	−0.349	−0.794	−0.708	−0.452	−0.667	−0.049	−0.444	−0.410	−0.523
MODSI2	0.529	0.546	0.713	0.681	0.846	0.333	0.576	−0.351	0.909
MODIS3	−0.409	−0.620	−0.519	−0.369	−0.692	0.015	−0.412	−0.610	−0.417
MODIS5	0.025	0.329	0.354	0.671	0.491	0.358	0.122	−0.641	0.627
NDVI	0.769	0.821	0.753	0.550	0.729	0.288	0.505	0.301	0.795
RDVI	0.828	0.797	0.766	0.580	0.766	0.318	0.535	0.218	0.864
EVI	0.827	0.776	0.764	0.605	0.761	0.313	0.550	0.062	0.869
MSAVI	0.842	0.781	0.758	0.581	0.776	0.324	0.546	0.193	0.877
SIPI	−0.748	−0.832	−0.833	−0.605	−0.629	−0.243	−0.475	0.090	−0.693

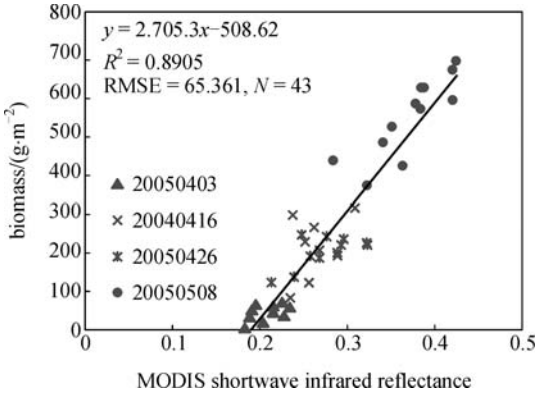

Fig. 9 Relation between biomass and MODIS shortwave infrared reflectance during vegetative stage

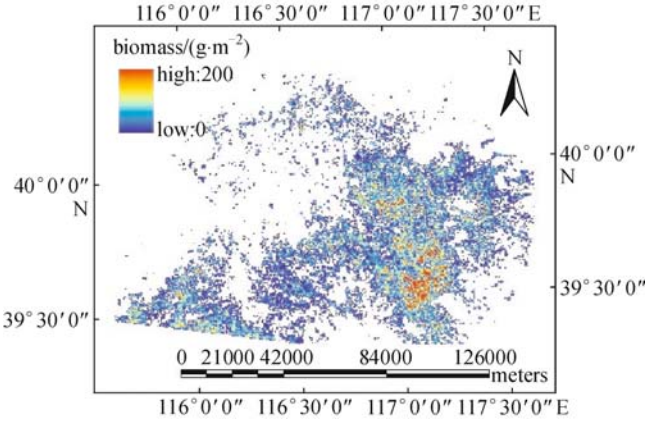

Fig. 11 Biomass map on April 17, 2004

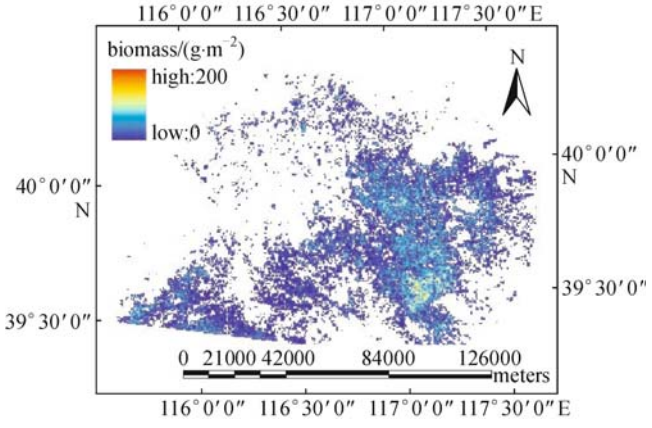

Fig. 10 Biomass map on April 1, 2004

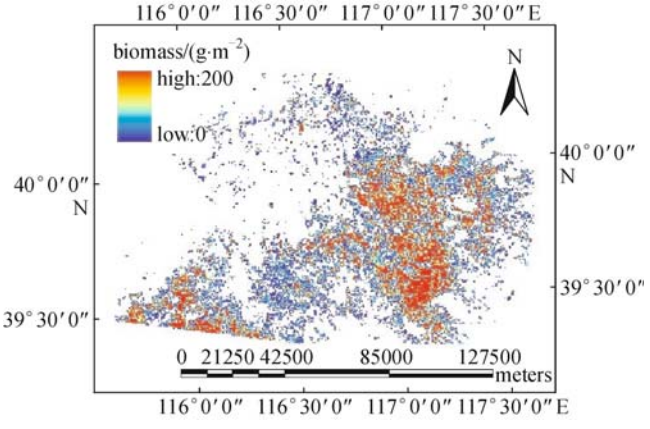

Fig. 12 Biomass map on May 6, 2005

coefficients change in regularity was comparable to the results from the TM analyses. During the vegetative stage, near infrared reflectance was the optimal index to estimate the wheat biomass.

(5) The relation between the biomass and near infrared reflectance could be best-fitted by a linear function based on the data generated during the vegetative stage. The model had a R^2 of 0.8905 with a RMSE of 65.361 g/m^2. Biomass estimation accuracy based on MODIS data was similar, with biomass estimation accuracy based on TM data. In searching the optimal spectral indices for estimating the wheat biomass, we found the optimal

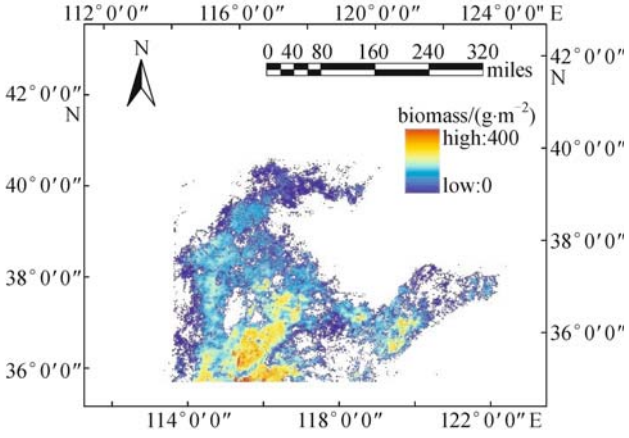

Fig. 13 Biomass map on March 29, 2004

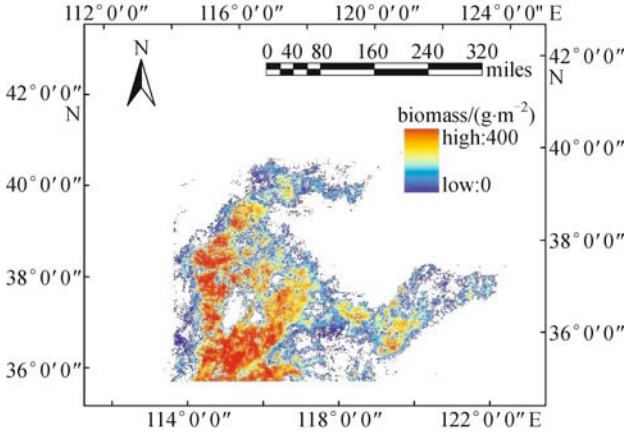

Fig. 14 Biomass map on April 14, 2004

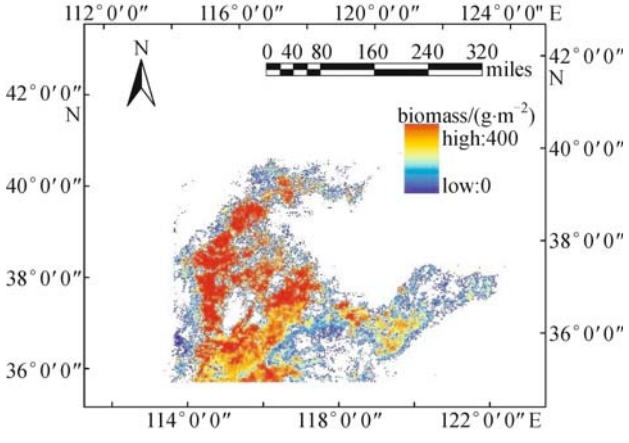

Fig. 15 Biomass map on May 8, 2005

indices of TM and MODIS were different. This result was due to differences in the SNR sensor and image pixel spatial resolution.

Acknowledgements This work was supported by the National Natural Science Foundation of China (Grant Nos. 40701130, 50721006), USDA CSREES (No. 2006–34263–16926), and National 973 Key Project of China (No. 2006CB403404), and Nanjing University of Information Science and Technology scientific research foundation.

References

Bao Y S (2006). Research of monitoring winter wheat growth using multi-source remote sensing data. Dissertation. Beijing: Bejing Normal University (in Chinese)

Baret F, Jacquemoud S, Guyot G, Leprieur C (1992). Modeled analysis of the biophysical nature of spectral shifts and comparison with information content of broad bands. Remote Sensing of Environment, 41(2—3): 133–142

Bonham-Carter G F (1988). Numerical procedures and computer program for fitting an inverted-Gaussian model to vegetation reflectance data. Computers and Geosciences, 14: 339–356

Buschmann C, Nagel E (1993). In vivo spectroscopy and internal optics of leaves as basis for remote sensing of vegetation. International Journal of Remote Sensing, 14: 711–722

Cho M A, Skidmore A K, Atzberger C (2008). Towards red-edge positions less sensitive to canopy biophysical parameters for leaf chlorophyll estimation using properties optique spectrales des feuilles (PROSPECT) and scattering by arbitrarily inclined leaves (SAILH) simulated data. International Journal of Remote Sensing, 29(8): 2241–2255

Clevers J G P W, De Jong S M, Epema G F, Van Der Meer F D, Bakker W H, Skidmore A K, Scholte K H (2002). Derivation of the red edge index using the MERIS standard band setting. International Journal of Remote Sensing, 23(16): 3169–3184

Collins W, Raines G L, Canney F C (1977, November 7–9). Airborne spectroradiometer discrimination of vegetation anomalies over sulphide mineralisation—a remote sensing technique. In: Abstract with Programmes. Seattle, Washington: Geological Society of America, 932–933

Colombo R, Meroni M, Marchesi A, Busetto L, Rossini M, Giardino C, Panigada C (2008). Estimation of leaf and canopy water content in poplar plantations by means of hyperspectral indices and inverse modeling. Remote Sensing of Environment, 112(4): 1820–1834

Curran P J (1989). Remote sensing of foliar chemistry. Remote Sensing of Environment, 30: 271–278

Curran P J, Windham W R, Gholz H L (1995). Exploring the relationship between reflectance red edge and chlorophyll concentration in slash pine leaves. Tree Physiology, 15: 203–206

Dawson T P, Curran P J (1998). A new technique for interpolating red edge position. International Journal of Remote Sensing, 19: 2133–2139

Del Frate F, Wang L F (2001). Sunflower biomass estimation using a scattering model and a neural network algorithm. International journal of remote sensing, 22(7): 1235–1244

Gao B C (1996). NDWI—a normalized difference water index for remote sensing of vegetation liquid water from space. Remote Sens Environ, 58: 257–266

Gates D M, Keegan H J, Schleter J C, Weidner V R (1965). Spectral properties of plants. Applied Optics, 4(1): 11–20

Ge S K, Xu M, Anderson G L, Carruthers R I (2007). Estimating Yellow Starthistle (*Centaurea solstitialis*) leaf area index and aboveground biomass with the use of hyperspectral data. Weed Scince,55(6): 671–678

Gitelson A A, Vina A, Arkebauer T J, Rundquist D C, Keydan G, Leavitt B (2003). Remote estimation of leaf area index and green leaf biomass in maize canopies. Geophysical Research Letters, 30(5): 1248, doi:10.1029/2002GL016450, 52–1—52–4

Horler D N H, Dockray M, Barber J (1983). The red edge of plant leaf reflectance. International Journal of Remote Sensing, 4: 273–288

Huang W J, Wang J H, Wang Z J, Jiang Z C, Liu L Y, Wang J D (2004). Inversion of foliar biochemical parameters at various physiological stages and grain quality indicators of winter wheat with canopy reflectance. International Journal of Remote Sensing, 25(12): 2409–2419

Huete A R, Liu H Q, Batchily K, van Leeuwen W (1997). A comparison of vegetation indices over a global set of TM images for EOS-MODIS, Remote Sensing of Environment59: 440–451

Jensen A, Lorenzen B, Spelling-Ostergaard H, Kloster-Hvelplund E (1990). Radiometric estimation of biomass and N content of barley grown at different N levels. International Journal of Remote Sensing,11: 1809–1820

Jin Y Q, Liu C (1997). Biomass retrieval from high-dimensional active/passive remote sensing data by using artificial neural networks. International journal of remote sensing, 18(4): 971–979

van Keulen H, Goudriaan J, Seligman N G (1989). Modelling the effects of nitrogen canopy development and crop growth. In: Russell G, Marshall B, Jarvis P G, eds. Plant Canopies: Their Growth Form and Function. Cambridge: Cambridge University Press, 83–104

Liu L Y (2002). Hyperspectral Remote Sensing Application in Precision Agriculture. Postdoctoral Report, 42–45

Liu L Y, Wang J H, Huang W J, Zhao C J, Zhang B (2004). Estimating winter wheat plant water content using red edge parameters. International Journal of Remote Sensing, 25(17): 3331–3342

Liu S F, Liou Y, Wang W J (2002). Retrieval of crop biomass and soil moisture from measure 1.4 and 10.65 GHz brightness temperatures. IEEE Transactions on Geoscience and Remote Sensing, 40(6): 1260–1268

Miller J R, Hare E W, WU J (1990). Quantitative characterization of vegetation red edge reflectance 1. An inverted-Gaussian reflectance model. International Journal of Remote Sensing, 11: 1755–1773

Penuelas J, Baret F, Filella I (1995). Semi-empirical indices to assess carotenoids/chlorophyll a ratio from leaf spectral reflectance. Photosynthetica 31: 221–230

Qi J, Chehbouni A, Huete A R, Keer Y H, Sorooshian S (1994). A modified soil vegetation adjusted index. Remote Sens. Environ. 48: 119–126

Railyan V Y, Korobov R M (1993). Red edge structure of canopy reflectance spectra of triticale. Remote Sensing of Environment, 46: 173–182

Rougean J L, Breon F M (1995). Estimating PAR absorbed by vegetation from bidirectional reflectance measurements. Remote Sens. Environ. 51: 375–384

Rouse J W, Haas R H, Schell J A, Deering D W, Harlan J C (1974). Monitoring the vernal advancements and retrogradation of natural vegetation. NASA/GSFC, Greenbelt, MD

Starks P J, Zhao D, Brown M A (2008). Estimation of nitrogen concentration and in vitro dry matter digestibility of herbage of warm-season grass pastures from canopy hyperspectral reflectance measurements. Grass and Forage Science, 63: 168–178

Svoray T (2002). SAR-based estimation of areal above ground biomass (AAB) of herbaceous vegetation in the semi-arid zone: a modification of the water-cloud model. International Journal of Remote Sensing, 23(19): 4089–4100

Tilling A K, O'Learyb G J, Ferwerdaa J G, Jonesa S D , Fitzgeraldb G J, Rodriguezc D, Belford R (2007). Remote sensing of nitrogen and water stress in wheat. Field Crops Research, 104(1–3): 77–85

Vuolo F, Dini L, D'Urso G (2008). Retrieval of leaf area index from CHRIS/PROBA data: an analysis of the directional and spectral information content. International Journal of Remote Sensing, 26 (17–18): 5063–5072

Wu C Y, Niu Z, Tang Q, Huang W J (2008). Estimating chlorophyll content from hyperspectral vegetation indices: modeling and validation. Agricultural and Forest Meteorology, 148(8–9): 1230–1241

Zarco-Tejada P J, Berjon A, Lopez-Lozano R, Miller J R, Martin P, Cachorro V, Gonzalez M R, De Frutos A (2005). Assessing vineyard condition with hyperspectral indices: Leaf and canopy reflectance simulation in a row-structured discontinuous canopy. Remote Sensing of Environment, 99(3): 271–287